

Migration of weakly bonded oxygen atoms in a-IGZO thin films and the positive shift of threshold voltage in TFTs

Chen Wang(王琛), Wenmo Lu(路文墨), Fengnan Li(李奉南), Qiaomei Luo(罗巧梅), and Fei Ma(马飞))
Citation: Chin. Phys. B, 2022, 31 (**9**): 096101. DOI: 10.1088/1674-1056/ac560f
Journal homepage: http://cpb.iphy.ac.cn; http://iopscience.iop.org/cpb

What follows is a list of articles you may be interested in

Spatial correlation of irreversible displacement in oscillatory-sheared metallic glasses

Shiheng Cui(崔世恒), Huashan Liu(刘华山), and Hailong Peng(彭海龙)
Chin. Phys. B, 2022, 31 (**8**): 086108. DOI: 10.1088/1674-1056/ac65f3

Combined effects of cycling endurance and total ionizing dose on floating gate memory cells

Si-De Song(宋思德), Guo-Zhu Liu(刘国柱), Qi He(贺琪), Xiang Gu(顾祥), Gen-Shen Hong(洪根深), and Jian-Wei Wu(吴建伟)
Chin. Phys. B, 2022, 31 (**5**): 056107. DOI: 10.1088/1674-1056/ac3d80

Effect of heavy ion irradiation on the interface traps of AlGaN/GaN high electron mobility transistors

Zheng-Zhao Lin(林正兆), Ling Lü(吕玲), Xue-Feng Zheng(郑雪峰), Yan-Rong Cao(曹艳荣), Pei-Pei Hu(胡培培), Xin Fang(房鑫), and Xiao-Hua Ma(马晓华)
Chin. Phys. B, 2022, 31 (**3**): 036103. DOI: 10.1088/1674-1056/ac11e4

Influences of total ionizing dose on single event effect sensitivity in floating gate cells

Ya-Nan Yin(殷亚楠), Jie Liu(刘杰), Qing-Gang Ji(姬庆刚), Pei-Xiong Zhao(赵培雄), Tian-Qi Liu(刘天奇), Bing Ye(叶兵), Jie Luo(罗捷), You-Mei Sun(孙友梅), Ming-Dong Hou(侯明东)
Chin. Phys. B, 2018, 27 (**8**): 086103. DOI: 10.1088/1674-1056/27/8/086103

Radiation damage effects on power VDMOS devices with composite SiO_2–Si_3N_4 films

Gao Bo, Liu Gang, Wang Li-Xin, Han Zheng-Sheng, Song Li-Mei, Zhang Yan-Fei, Teng Rui, Wu Hai-Zhou
Chin. Phys. B, 2013, 22 (**3**): 036103. DOI: 10.1088/1674-1056/22/3/036103

Migration of weakly bonded oxygen atoms in a-IGZO thin films and the positive shift of threshold voltage in TFTs

Chen Wang(王琛), Wenmo Lu(路文墨), Fengnan Li(李奉南), Qiaomei Luo(罗巧梅), and Fei Ma(马飞)†

State Key Laboratory for Mechanical Behavior of Materials, Xi'an Jiaotong University, Xi'an 710049, *China*

(Received 1 December 2021; revised manuscript received 29 January 2022; accepted manuscript online 17 February 2022)

Amorphous indium-gallium-zinc oxide (a-IGZO) thin films are prepared by pulsed laser deposition and fabricated into thin-film transistor (TFT) devices. *In-situ* x-ray photoelectron spectroscopy (XPS) illustrates that weakly bonded oxygen (O) atoms exist in a-IGZO thin films deposited at high O_2 pressures, but these can be eliminated by vacuum annealing. The threshold voltage (V_{th}) of the a-IGZO TFTs is shifted under positive gate bias, and the V_{th} shift is positively related to the deposition pressure. A temperature variation experiment in the range of 20 K–300 K demonstrates that an activation energy of 144 meV is required for the V_{th} shift, which is close to the activation energy required for the migration of weakly bonded O atoms in a-IGZO thin films. Accordingly, the V_{th} shift is attributed to the acceptor-like states induced by the accumulation of weakly bonded O atoms at the a-IGZO/SiO_2 interface under positive gate bias. These results provide an insight into the mechanism responsible for the V_{th} shift of the a-IGZO TFTs and help in the production of reliable designs.

Keywords: a-IGZO thin films, weakly bonded O atoms, threshold voltage shift

PACS: 61.43.Dq, 68.35.Fx, 85.30.Tv **DOI:** 10.1088/1674-1056/ac560f

1. Introduction

The development of high-resolution and flexible display technology depends heavily on the channel materials of thin-film transistors (TFTs). Amorphous indium-gallium-zinc oxide (a-IGZO) has attracted much attention due to its high mobility and potential application in flexible devices.[1–3] However, the shift of threshold voltage (V_{th}) of a-IGZO TFTs under positive gate bias is still a critical issue. The positive V_{th} shift in TFTs has been ascribed to the negative charges accumulated at the a-IGZO/insulator interface and the screened gate electric field.[4–7] The negative charges could come from electrons trapped in the gate dielectrics[8] or acceptor-like states. Electron trapping in gate dielectrics commonly occurs in TFTs with high-permittivity gate dielectrics, so it is not widespread. Nomura *et al.* attributed the V_{th} shift to shallow trap states.[9] Chowdhury *et al.* carried out a time–temperature dependence experiment, and attributed the V_{th} shift to defects corresponding to the fitted activation energy, but the fitting accuracy was limited by the narrow temperature range (27 °C–90 °C).[10] Um *et al.* observed a hump in the subthreshold region of the transfer curves under positive gate bias, and ascribed it to the acceptor-like states near the a-IGZO/insulator interface.[11] Apparently, the mechanism for the V_{th} shift is still controversial. Furthermore, those mechanisms cannot be adopted to explain the effect of ambient O_2 on the V_{th} shift. To understand the ambient effect, Zhou *et al.* proposed a model of chemically adsorbed O_2.[12] Chen *et al.* found that the activation energy of O_2 adsorption could be lowered by gate bias, resulting in a V_{th} shift in an O_2 atmosphere.[13] Xu *et al.* illustrated that the ambient O_2 could compensate for the oxygen vacancies and improve the subthreshold performance.[14] In other words, a contradiction still exists regarding the effect of ambient O_2, and it is still not understood why and how the adsorption of O_2 at the back channel can induce acceptor-like states at the a-IGZO/insulator interface.

In this work, a-IGZO thin films are prepared by pulsed laser deposition (PLD) and are fabricated into TFT devices. The morphology, phase structure, and chemical states of the a-IGZO thin films are characterized, and the influences of the deposition O_2 pressure, vacuum annealing temperature, ambient O_2, and film thickness on the electrical properties of the a-IGZO TFTs are investigated; in particular, the V_{th} shift under positive gate bias is discussed. Furthermore, *in-situ* x-ray photoelectron spectroscopy (XPS), a temperature variation experiment and an *in-situ* vacuum annealing experiment were carried out to understand the mechanism responsible for the V_{th} shift of the a-IGZO TFTs. It was found that the V_{th} shift could be attributed to the deep acceptor-like states induced by the accumulation of weakly bonded O atoms at the a-IGZO/SiO_2 interface.

2. Experiment

2.1. Preparation and characterization of a-IGZO thin films

The a-IGZO thin films are prepared by the pulsed laser deposition (PLD) technique using a KrF excimer laser (248 nm, ∼ 10 J·cm^{-2} per pulse). The target is a home-made crystalline IGZO ceramic (In : Ga : Zn : O = 2 : 2 : 1 : 7 mol%) sintered at 1400 °C. The surface morphology of the

†Corresponding author. E-mail: mafei@mail.xjtu.edu.cn

© 2022 Chinese Physical Society and IOP Publishing Ltd

a-IGZO thin films is observed using a scanning electron microscope (SEM) and the phase structure is characterized by x-ray diffraction (XRD, $\lambda = 1.5406$ Å). An interconnected XPS and PLD system in a vacuum chamber is used for *in-situ* characterization of the elemental contents and chemical states to avoid contaminants and adsorbates. The excitation source for the XPS is Al $K\alpha$ with an energy of 1486.6 eV. The sample is heated in an analysis chamber, which has a better vacuum than 1.0×10^{-5} Pa. The XPS spectra of O 1s in the interior and on the surface of the thin film are measured by changing the photoelectron collection angle from 90° to 30°.

2.2. Fabrication of TFTs and details of the electrical measurement

The a-IGZO TFTs with a top contact and a bottom gate (p^+-Si substrate) are fabricated. The insulator consists of 280 nm of thermally oxidized SiO_2, and 100 nm Mo source/drain electrodes are deposited by radio frequency (RF) magnetron sputtering. *In-situ* electrical measurements of the TFTs are carried out using a homemade probe station in vacuum. The probe station is pumped by a molecular pump unit. Pure O_2 gas can be introduced into the station. Alumina ceramic heating plates and K-type thermal sensors are attached to the samples and the temperature is regulated by an Eurotherm 3504 controller. In this setup, four samples can be measured at the same time by a combination of a Keithley 2700 matrix switcher and a 2612b source meter. The transfer curves can be measured after thermal annealing in a vacuum better than 10^{-4} Pa. The temperature variation measurements are implemented in a He exchange cryostat. The sample is cooled by the circulation of helium around a closed circuit driven by a dry pump. The helium gas is cooled by the cryo cooler to the 40 K and 4 K stages and then cooled further via expansion from the needle valve. A heat exchanger is used to adjust the temperature of the helium gas, and thus the sample temperature is controlled in the range of 20 K–300 K. All the electric measurements are done in the dark.[15,16]

Transfer curves are measured by sweeping V_g from −60 V to 60 V in steps of 0.5 V, with V_d kept at 2 V. To evaluate the V_{th} shift, a constant gate voltage (V_g) of 60 V and a drain voltage (V_d) of 2 V are biased for 400 s after each transfer curve measurement. For the recovery process, the a-IGZO TFTs are electrically disconnected for 400 s and the V_g sweeping is stopped when I_d is larger than 5 nA, taking the turn-on voltage (V_{on}) shift to represent the V_{th} shift. The V_{th} is calculated through the transfer curve

$$I_d = \frac{\mu W C_{ox}}{L}\left(V_g - V_{th}\right)V_d, \tag{1}$$

in which L and W are the channel length and width, respectively, C_{ox} is the unit area capacitance of the insulator dielectrics, and V_d is the drain voltage. V_{th} is determined by fitting the linear region of the I_d–V_g curves. The field effect mobility (μ) is obtained by fitting the linear region of the transfer curves

$$\mu = \frac{L}{WC_{ox}V_d}\frac{\partial I_d}{\partial V_g}. \tag{2}$$

2.3. Grünewald method

The Grünewald method is adopted to extract the density of states (DOS) of a-IGZO from the transfer curves. The starting point for this method is the 1D Poisson equation

$$\frac{\partial^2 V(x)}{\partial x^2} = -\frac{en(x)}{\varepsilon_0 \varepsilon_S}, \tag{3}$$

in which $V(x)$ is the electrostatic potential at position x in a-IGZO, e is the elementary charge, $n(x)$ is the total charge density, ε_0 is the vacuum permittivity and ε_S is the dielectric constant. The current in the a-IGZO films is integrated along the thickness

$$I = \frac{I_0}{d}\int_0^d \exp\left(\frac{eV(x)}{k_B T}\right)\mathrm{d}x, \tag{4}$$

in which d is the thickness of a-IGZO, I_0 is the flat band current, k_B is the Boltzmann constant, and T is the temperature. The boundary conditions of the 1D Poisson equation are

$$\varepsilon_0\varepsilon_{ox}\frac{V_g - V_{FB}}{l} = -\varepsilon_0\varepsilon_S\frac{\partial V(x)}{\partial x}|_{x=0}, \tag{5}$$

$$V(d) = 0, \quad \frac{\partial V(x)}{\partial x}|_{x=d} = 0, \tag{6}$$

in which ε_{ox} is the dielectric constant of the gate insulator, V_g is the gate voltage, V_{FB} is the flat band voltage, and l is the thickness of the gate insulator. The surface potential of the a-IGZO thin films can be calculated by solving the equation below:

$$\exp\left(\frac{eV_0}{k_B T}\right) - \frac{eV_0}{k_B T} - 1 = \frac{e}{k_B T}\frac{\varepsilon_{ox} d}{\varepsilon_S l I_0} \times\left(\left(V_g - V_{FB}\right)\times I\left(V_g - V_{FB}\right) - \int_0^{V_g - V_{FB}} I\left(V_g'\right)\mathrm{d}V_g'\right). \tag{7}$$

The gate voltage V_g and the total density can then be calculated by

$$n(V_0) = \frac{\varepsilon_{ox}^2\varepsilon_0}{\varepsilon_S l^2 e}\left(V_g - V_{FB}\right)\left(\frac{\partial V_0}{\partial\left(V_g - V_{FB}\right)}\right)^{-1}. \tag{8}$$

The DOS can be extracted from the transfer curves and the flat band voltage

$$\frac{1}{e}\frac{\mathrm{d}n(V_0)}{\mathrm{d}V_0} = \mathrm{DOS}(E_F + eV_0). \tag{9}$$

The flat band voltage is considered to be approximately equal to V_{on} when the source–drain current is 5 nA. The extraction of the DOS is carried out in Matlab.

3. Results and discussion

3.1. Characterization of the a-IGZO thin films

Figure 1 shows SEM images of the a-IGZO thin films. Evidently, the film surface is smooth if the deposition pressure is lower than 6 Pa, but clusters appear on the surface at a deposition pressure of 10 Pa, and the thin films become rough. Therefore, deposition pressures in the range of 2.0 Pa–4.5 Pa can avoid the influence of surface roughness. Figure 2 shows XRD patterns of a-IGZO thin films deposited at oxygen pressures of 1 Pa–10 Pa and annealed at 373 K–873 K. As displayed in Fig. 2(a), no sharp peak can be identified in the patterns, confirming the deposition-pressure-independent amorphous characteristic of a-IGZO. Furthermore, as shown in Fig. 2(b), the amorphous structure can be thermally stable at up to 673 K. Therefore, the effects of phase structure and transition on the electric performance can also be excluded.

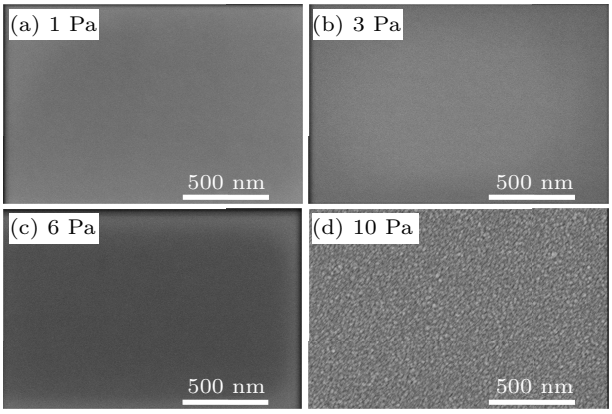


Fig. 1. SEM images of a-IGZO thin films deposited at different O_2 pressures: (a) 1 Pa, (b) 3 Pa, (c) 6 Pa, and (d) 10 Pa.

To further understand the influence of deposition pressure and vacuum annealing on the a-IGZO films, *in-situ* XPS is carried out, and the results are shown in Fig. 3. The O 1s spectrum is deconvoluted by the Voight function into two peaks at 531.0 eV (the O_I peak) and ∼ 532.5 (±0.1) eV (the O_{II} peak) in Fig. 3(a). A peak (peaks) corresponding to surface impurities is (are) not in evidence; in other words, *in-situ* characterization can avoid the influences of surface impurities on the O1s spectrum. The O_I peak originates from the lattice oxygen atoms, which are tightly bonded with surrounding In atoms in the form of In–O_6.[17] As shown in Fig. 3(b), the O content of IGZO thin films deposited at oxygen pressures of 1 Pa–5 Pa oxygen pressure is greater than 58.3% (corresponding to the stoichiometric ratio in $In_2Ga_2ZnO_7$), indicating the presence of excess O atoms in a-IGZO thin films. The bond length between the weakly bonded O atoms and the surrounding In atoms is considerably larger than the normal In–O bond (0.211 nm), with less charge transfer from In to O atoms and thus a higher binding energy of O 1s.[18] Therefore, the O_{II} peak originates from the weakly bonded O atoms rather than

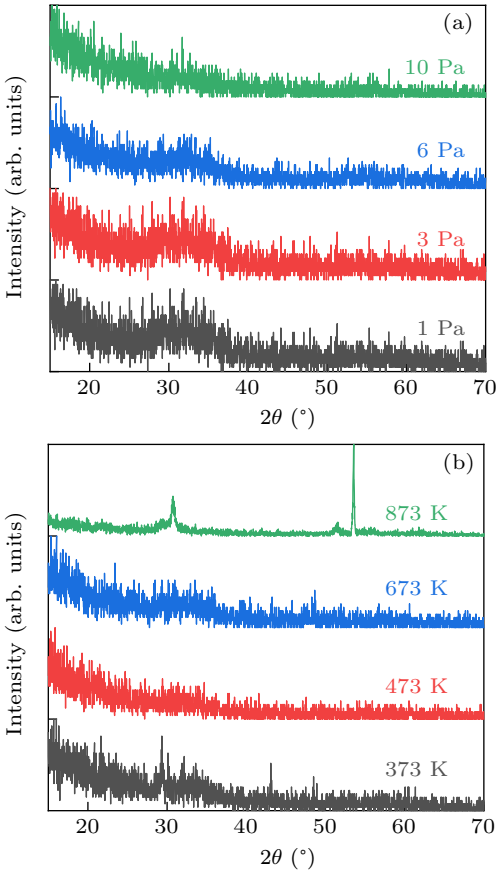


Fig. 2. (a) XRD patterns of a-IGZO thin films deposited at different O_2 pressures, namely, 1 Pa, 3 Pa, 6 Pa, and 10 Pa. (b) XRD patterns of a-IGZO films deposited at a pressure of 3 Pa of O_2 and annealed at 373 K, 473 K, 673 K, and 873 K in vacuum for 12 hours.

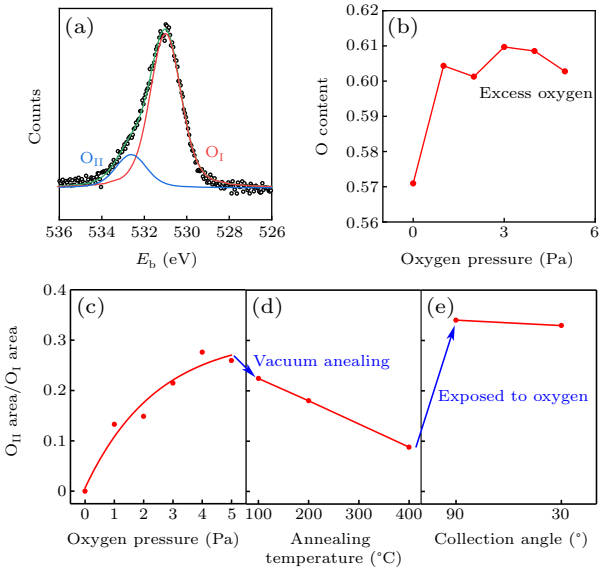


Fig. 3. *In situ* XPS analysis of a-IGZO films. (a) O 1s spectrum of a-IGZO deposited at a pressure of 3.0 Pa of O_2. (b) The O content and (c) the area ratio of O_{II}/O_I in a-IGZO thin films deposited at different O_2 pressures. (d) The area ratio of O_{II}/O_I in a-IGZO thin films deposited at a pressure of 5 Pa of O_2 and annealed at different temperatures. (e) The area ratio of O_{II}/O_I in a-IGZO thin films deposited at a pressure of 5 Pa of O_2, collected at 90° and 30°, and then annealed at 400 °C.

oxygen vacancies. The content of weakly bonded O atoms increases with the deposition pressure (Fig. 3(c)), but decreases with increasing annealing temperature in vacuum (Fig. 3(d)).

The content of weakly bonded O atoms both in the interior and on the surface increases once the annealed a-IGZO thin films are exposed to 10^5 Pa ambient O_2 for 12 hours (Fig. 3(e)). Therefore, the increment of weakly bonded O atoms is caused by the migration of ambient O_2 into the a-IGZO thin films, but not by the adsorption of O_2.

3.2. The influence of deposition pressure on the V_{th} shift

Figure 4(a) schematically displays the cross-section of the a-IGZO TFTs. Figure 4(b) shows the output curves of a-IGZO TFTs deposited at an oxygen pressure of 3.0 Pa, and the TFTs are in the linear region at a V_d of 2 V. Figure 5 shows the transfer curves of a-IGZO TFTs under positive gate bias. The V_{th} shift is evidenced in all the a-IGZO TFTs, and increases remarkably with deposition pressure. As mentioned above, the number of weakly bonded O atoms also increases with the deposition pressure. On the whole, the V_{th} shift might be ascribed to the acceptor-like states induced by the weakly bonded O atoms.[19] In essence, the V_{th} shift occurs if electrons are trapped in acceptor-like states.

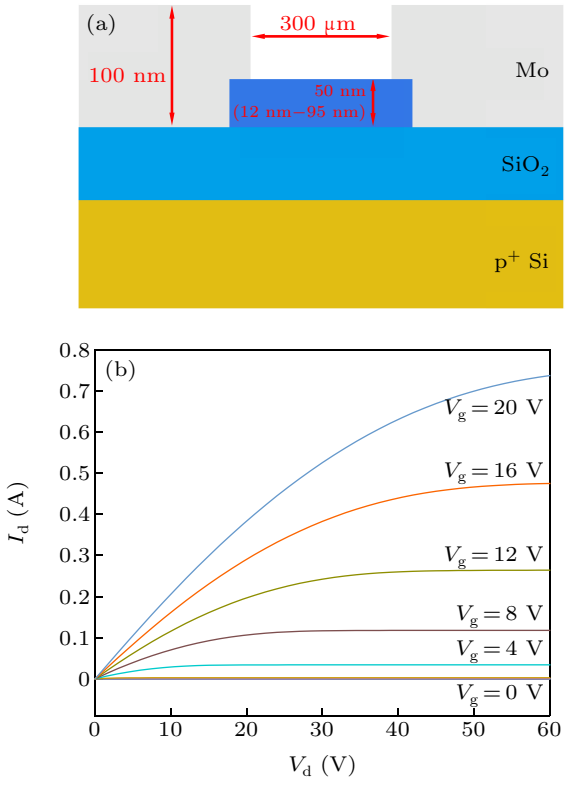


Fig. 4. (a) Schematic cross-section of a-IGZO TFTs. (b) Output curves of an a-IGZO TFT deposited at a pressure of 3 Pa of O_2.

3.3. Temperature variation experiment

A temperature variation experiment is carried out to study the thermally activated process of the V_{th} shift. As shown in Fig. 6(a), the TFTs exhibit normal transfer curves at 20 K–300 K, both the mobility and V_{on} change significantly for temperatures of 200 K or less, but are almost temperature independent at 200 K–300 K (Fig. 6(b)). A series of transfer curves are measured under positive gate bias and at different temperatures. The difference between the V_{th} values with and without bias (ΔV_{th}) is used to quantitatively describe the V_{th} shift. As displayed in Figs. 6(c) and 6(d), the V_{th} shift is thermally activated, and the temperature-dependent V_{th} shift is a good fit for an activation model, i.e., $\Delta V_{th} = A\exp(-E_a/kT)$. The activation energies of the V_{th} shift and the recovery process are fitted to 144 meV and 195 meV, which are close to the activation energy of oxygen diffusion in a-IGZO ($\sim$ 100 meV).[20] Accordingly, it is proved that the V_{th} shift of a-IGZO TFTs is induced by the accumulation of weakly bonded O atoms at the a-IGZO/SiO_2 interface under positive gate bias. It should be noted that the migration of weakly bonded O atoms is not significant at 200 K or below, and thus the V_{th} shift at low temperature is mainly controlled by the electrons trapped in the pre-existing acceptor-like states, which have quite small thermal activation energies.

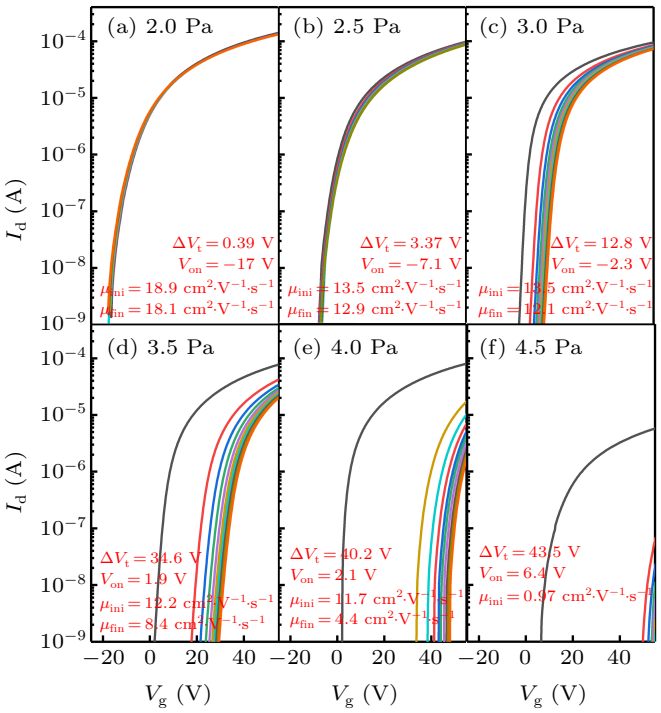


Fig. 5. Transfer curves (I_d–V_g) of a-IGZO TFTs with 50 nm a-IGZO thin films deposited at different O_2 pressures and measured under positive gate bias.

3.4. The influences of ambient O_2 on the V_{th} shift

Ambient O_2 could also induce the V_{th} shift.[12–14,21] *In-situ* vacuum annealing and measurement are implemented to study the influence of ambient O_2 on the V_{th} shift by allowing O_2 at different pressures into the vacuum chamber after *in-situ* annealing. Figure 7 displays the transfer curves of a-IGZO TFTs annealed at 383 K–398 K in a better vacuum than 10^{-4} Pa for 12 hours. A remarkable V_{th} shift occurs in the TFTs annealed at 383 K, while deteriorated subthreshold performance is observed in the TFTs annealed at 393 K and 398 K because of the large number of oxygen vacancies induced by vacuum annealing at higher temperatures. Accordingly, 388 K

is the optimal vacuum annealing temperature. Figure 8 shows the transfer curves of TFTs with 10 nm IGZO films deposited at an oxygen pressure of 3.0 Pa and annealed at 388 K, then exposed to O_2 at a pressure of 10^{-4} Pa–10^5 Pa. Since the film thickness is smaller than the Debye length in the subthreshold region ($\sim$ 11 nm), the effect of adsorbed O_2 can be observed in the transfer curves.[12] After vacuum annealing, the mobility of the TFTs is remarkably improved from 13.5 $cm^2 \cdot V^{-1} \cdot s^{-1}$ to 31.4 $cm^2 \cdot V^{-1} \cdot s^{-1}$. Compared with the deposited TFTs, the TFTs annealed in vacuum at a pressure of 10^{-4} Pa do not exhibit the V_{th} shift, indicating that the weakly bonded O atoms are eliminated, which is also confirmed by the *in situ* XPS. As the ambient O_2 pressure increases, V_{on} moves positively, even at low O_2 pressures, as a result of a depletion layer induced by O_2 adsorption.[22] However, a considerable V_{th} shift occurs only at high ambient O_2 pressures, which cannot be explained by O_2 adsorption. Taking this into account, it is further confirmed that the V_{th} shift of a-IGZO TFTs in ambient O_2 can be ascribed to the migration of weakly bonded O atoms from ambient O_2 into the a-IGZO thin films, as confirmed by the *in-situ* XPS spectra.

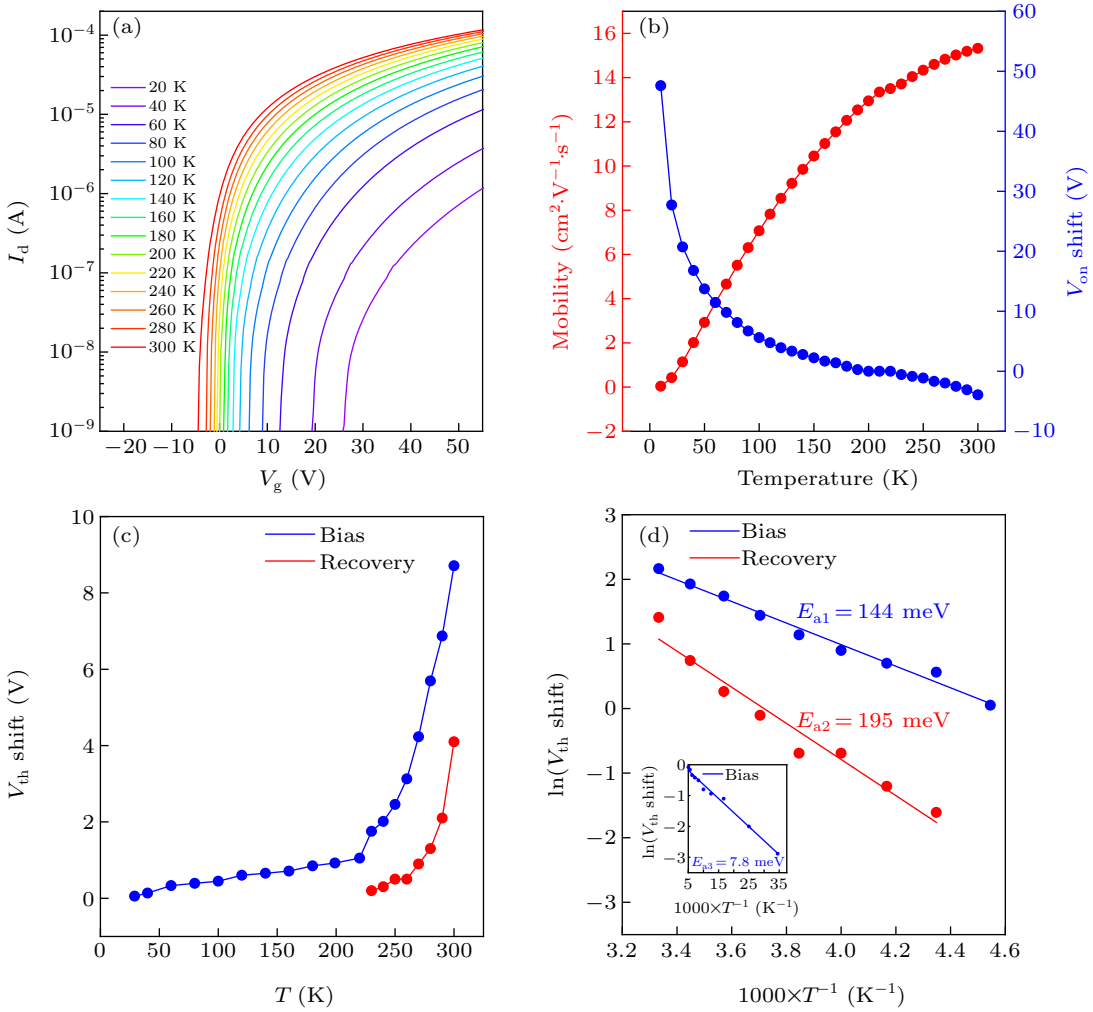


Fig. 6. Temperature dependence of transfer curves and the V_{th} shift. (a) Transfer curves at 20 K–300 K. (b) Field-effect mobility and turn-on voltage. (c) and (d) The V_{th} shift as a function of temperature in the bias and recovery processes in linear and logarithmic coordinates, respectively.

3.5. The migration of ambient O_2 controlled by the a-IGZO thickness

Given that the V_{th} shift is caused by the migration of ambient O_2, the thickness of the a-IGZO films might affect the V_{th} shift substantially. Thus, the V_{th} shift of TFTs with a-IGZO thicknesses of 12 nm–95 nm are fitted to a stretched exponential function[23]

$$\Delta V_{th}(t) = \Delta V_{inf}\left(1 - \exp\left(-\left(\frac{t}{\tau}\right)^{\beta}\right)\right), \tag{10}$$

in which ΔV_{inf} is the V_{th} shift at infinite time, t is the time, τ is the time constant, and β is the exponential factor. The fitted results are plotted in Fig. 9; ΔV_{inf} and τ are used to quantitatively describe the V_{th} shift. As the thickness of a-IGZO thin films is increased, ΔV_{inf} decreases and τ increases, suggesting a reduced V_{th} shift, which can be ascribed to the suppressed migration of ambient O_2 in the thicker a-IGZO films. A critical thickness of 50 nm is enough to avoid the influence of ambient O_2. The β value of 0.4 is maintained for different thicknesses,

which means that the migration of weakly bonded O atoms is dominated by a short-range force.[24]

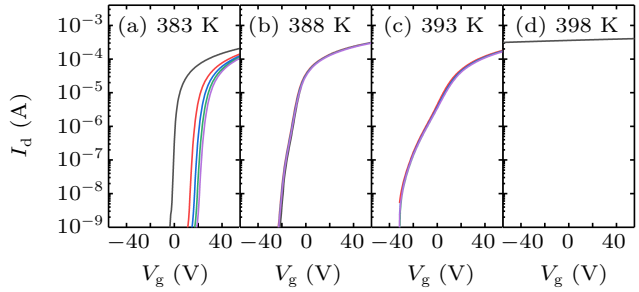


Fig. 7. Transfer curves (I_d–V_g) of 10 nm a-IGZO TFTs annealed in vacuum at different temperatures: (a) 383 K, (b) 388 K, (c) 393 K, and (d) 398 K.

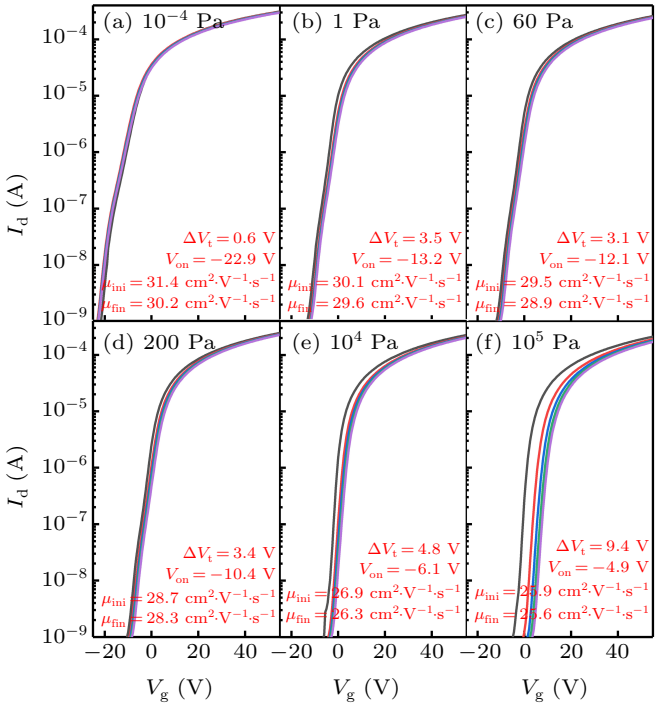


Fig. 8. Transfer curves (I_d–V_g) of 10 nm a-IGZO TFTs biased at different ambient O_2 pressures and measured under positive gate bias.

3.6. Deep acceptor-like states generated by weakly bonded O atoms

The acceptor-like states in a-IGZO can be divided into two types, shallow states and deep states.[25] The DOS of shallow states is extracted from the transfer curves using the Grünewald method,[26,27] and the results are plotted in Fig. 10. For a-IGZO films annealed in vacuum, the ionized oxygen vacancies (V_O^{2+}) induce shallow acceptor-like states at ~ 0.1 eV above the Fermi level,[28] as shown in Fig. 10(a). Oxygen vacancies affect the electrical properties of a-IGZO TFTs significantly, and can result in a negative V_{th} shift.[14,28] However, the positive V_{th} shift cannot be ascribed to oxygen vacancies (V_O). If the positive V_{th} shift is closely related to V_O, and V_O, as the shadow donors, could provide free carriers, the turn-on voltage should become more negative with a larger positive V_{th} shift at a higher oxygen vacancy concentration, which is in contradiction to the experimental results in this work. As shown in Figs. 5 and 8, if the a-IGZO thin films are deposited at lower oxygen pressures or exposed at lower ambient oxygen pressures, more V_O is involved, but the TFTs exhibit a more stable V_{th} under a positive gate bias. Therefore, the positive V_{th} shift is not directly related to oxygen vacancies. On the other hand, the carriers in TFTs are confined to a thin region (~ 1 nm) close to the dielectrics, and will be scattered by deep trapped electrons at the a-IGZO/SiO_2 interface. Therefore, the reduced mobility in Figs. 5 and 8 corresponds to the deep trapped electrons at the a-IGZO/SiO_2 interface.[19,29]

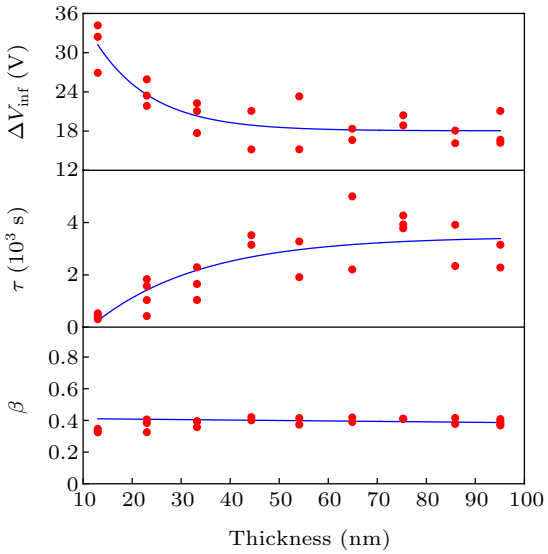


Fig. 9. The V_{th} shift of TFTs with different a-IGZO thicknesses tested in an O_2 atmosphere; the values of V_{th} at infinity (ΔV_{inf}), the time constant (τ), and the exponential factor (β) are extracted by fitting the stretched exponential equation.

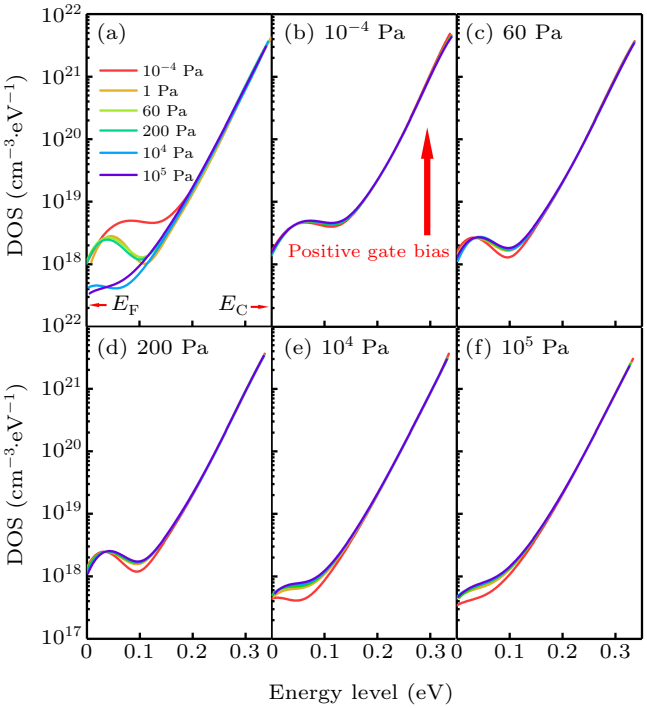


Fig. 10. Density of states (DOS) with respect to the Fermi level extracted by the Grünewald method. (a) DOS of TFTs before bias at different ambient O_2 pressures. (b)–(f) DOS of TFTs biased at 10^{-4} Pa, 60 Pa, 200 Pa, 10^4 Pa, and 10^5 Pa, respectively.

Figure 11 schematically shows a physical picture of the positive V_{th} shift in a-IGZO TFTs. As displayed in Figs. 11(a) and 11(b), the weakly bonded O atoms in the a-IGZO thin films migrate towards the a-IGZO/SiO_2 interface under a positive gate bias and induce deep acceptor-like states at the interface. The electrons trapped in the deep acceptor-like states will screen the gate field, leading to a potential step and the positive V_{th} shift. However, the oxygen-vacancy-related mechanism (Figs. 11(c) and 11(d)) cannot be adopted to adequately interpret the screening effect on the gate electric field.

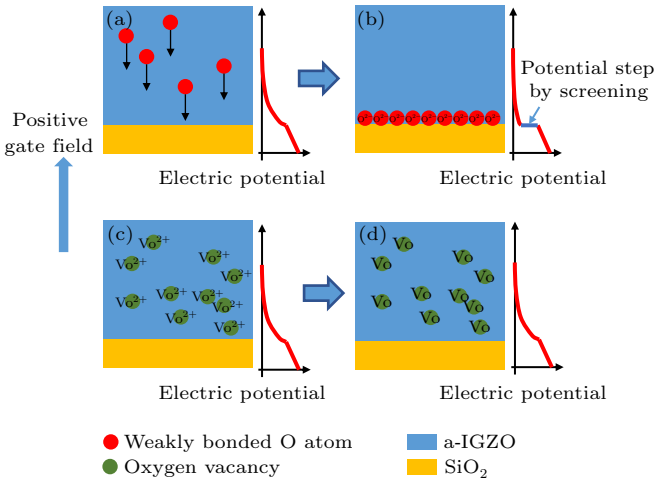


Fig. 11. Schematic diagram of the positive V_{th} shift in a-IGZO TFTs. (a) and (b) A model of the weakly bonded O atom migration under the gate electric field. (c) and (d) A model of ionized oxygen vacancies capturing electrons under the gate electric field.

4. Conclusion

In this work, a-IGZO thin films are prepared by PLD, and a-IGZO TFTs are fabricated. The morphology, phase structure, and chemical states of the a-IGZO thin films are characterized. *In-situ* XPS demonstrates that weakly bonded O atoms are induced in a-IGZO thin films at high deposition pressures, but can be eliminated by vacuum annealing. High deposition pressures lead to large V_{th} shifts, and the activation energy of the V_{th} shift is fitted to 144 meV as part of the temperature variation experiment. Accordingly, the V_{th} shift is caused by the generation of deep acceptor-like states due to the accumulation of weakly bonded O atoms at the a-IGZO/SiO_2 interface under positive gate bias. Furthermore, the V_{th} shift can also be caused by the migration of O atoms from ambient O_2 into a-IGZO, which can be suppressed if the IGZO film is thick enough. The results are helpful for the design of reliable IGZO TFTs and their potential applications in flexible displays.

Acknowledgments

Project supported by the National Natural Science Foundation of China (Grant Nos. 51771144 and 62104189), the Natural Science Foundation of Shaanxi Province, China (Grant Nos. 2021JC-06, 2019TD-020, and 2019JLM-30), the China Postdoctoral Science Foundation (Grant No. 2020M683483), and the Fundamental scientific research business expenses of Xi'an Jiaotong University (Grant No. XZY022020017).

References

[1] Zhang M N, Shao Y, Wang X L, Wu X, Liu W J and Ding S J 2020 *Chin. Phys. B* **29** 078503
[2] Zhang D, Wu C, Xu W, Ren F, Zhou D, Yu P, Zhang R, Zheng Y and Lu H 2019 *Chin. Phys. B* **28** 017303
[3] Nomura K, Ohta H, Takagi A, Kamiya T, Hirano M and Hosono H 2004 *Nature* **432** 488
[4] Powell M J, Van Berkel C and Hughes J R 1989 *Appl. Phys. Lett.* **54** 1323
[5] Gelatos A V and Kanicki J 1990 *Appl. Phys. Lett.* **57** 1197
[6] Libsch F R and Kanicki J 1993 *Appl. Phys. Lett.* **62** 1286
[7] Kakalios J, Street R A and Jackson W B 1987 *Phys. Rev. Lett.* **59** 1037
[8] Zafar S, Callegari A, Gusev E and Fischetti M V 2003 *J. Appl. Phys.* **93** 9298
[9] Nomura K, Kamiya T, Hirano M and Hosono H 2009 *Appl. Phys. Lett.* **95** 013502
[10] Chowdhury M D H, Migliorato P and Jang J 2011 *Appl. Phys. Lett.* **98** 153511
[11] Um J G, Mativenga M, Migliorato P and Jang J 2014 *J. Appl. Phys.* **115** 134502
[12] Zhou X, Shao Y, Zhang L, Xiao X, Han D, Wang Y and Zhang S 2017 *IEEE Electron Dev. Lett.* **38** 465
[13] Chen Y C, Chang T C, Li H W, Chen S C, Lu J, Chung W F, Tai Y H and Tseng T Y 2010 *Appl. Phys. Lett.* **96** 262104
[14] Xu J, Wu Q, Xu L, Xie H, Liu G, Zhang L and Dong C 2016 *Solid State Electron.* **126** 170
[15] Wang Y, Wang M, Zhang D and Wang H 2020 *Chin. Phys. B* **29** 118101
[16] Tang L F, Yu G, Lu H, Wu C F, Qian H M, Zhou D, Zhang R, Zheng Y D and Huang X M 2015 *Chin. Phys. B* **24** 088504
[17] Han S Y, Herman G S and Chang C H 2011 *J. Am. Chem. Soc.* **133** 5166
[18] Nomura K, Kamiya T, Ohta H, Uruga T, Hirano M and Hosono H 2007 *Phys. Rev. B* **75** 035212
[19] Han W H, Oh Y J, Chang K J and Park J S 2015 *Phys. Rev. Appl.* **3** 044008
[20] Nomura K, Kamiya T and Hosono H 2013 *ECS J. Solid State Sci. Technol.* **2** P5
[21] Liu P T, Chou Y T and Teng L F 2009 *Appl. Phys. Lett.* **95** 233504
[22] Kang D, Lim H, Kim C, Song I, Park J, Park Y and Chung J 2007 *Appl. Phys. Lett.* **90** 192101
[23] Jeong J, Lee G J, Kim J, Kim J and Choi B 2013 *Appl. Phys. Express* **6** 031101
[24] Phillips J C 1996 *Reports Prog. Phys.* **59** 1133
[25] Alkauskas A, McCluskey M D and Van De Walle C G 2016 *J. Appl. Phys.* **119** 181101
[26] Grünewald M, Thomas P and Würtz D 1980 *Phys. Status Solidi B* **100** 139
[27] Geiger M, Schwarz L, Zschieschang U, Manske D, Pflaum J, Weis J, Klauk H and Weitz R T 2018 *Phys. Rev. Appl.* **10** 044023
[28] Jang J T, Park J, Ahn B Du, Kim D M, Choi S J, Kim H S and Kim D H 2015 *ACS Appl. Mater. Interfaces* **7** 15570
[29] Wang X and Dodabalapur A 2018 *Ann. Phys.* **530** 1800341